

## Numerical Results for a Colocated Finite-Volume Scheme on Voronoi Meshes for Navier-Stokes Equations

V.C. Mariani<sup>1</sup>, E.E.M. Alonso<sup>2</sup> and S. Peters<sup>3</sup>

**Abstract:** An application of Newton's method for linearization of advective terms given by the discretization on unstructured Voronoi meshes for the incompressible Navier-Stokes equations is proposed and evaluated in this article. One of the major advantages of the unstructured approach is its application to very complex geometrical domains and the mesh is adaptable to features of the flow. Moreover, in this work comparisons with the literature results in bi-dimensional lid-driven cavities for different Reynolds numbers allow us to assess the numerical properties of the new proposed finite-volume scheme. Results for the components of the velocity, and the pressure colocated at the centers of the control volumes are presented and discussed. On the basis of the numerical experiments reported in this article it seems that the method under investigation has no difficulty at capturing the formation of primary and secondary vortices as Reynolds number increases.

**Keyword:** Newton method, Voronoi Diagram, Navier-Stokes equations, cavity.

### 1 Introduction

Approximate solutions for the Navier-Stokes equations have been extensively studied and various methods have already been presented in the literature. Traditionally, the finite difference methods have employed structured meshes, while

finite element methods have utilized unstructured meshes, already finite volume method has utilized both meshes. The relative advantages and disadvantages, from the viewpoint of computational fluid dynamics have been discussed in Weatherill (1992), Mishev (1998), and Li et al. (2000).

In engineering applications, various finite-volume method schemes have been used on Cartesian grids or orthogonal meshes, and the use of unstructured meshes have been developed mainly for compressible flows, while the developments for incompressible flows have been performed on structured meshes using marker-and-cell scheme (MAC) proposed originally by Harlow and Welch (1965), while MAC scheme to unstructured meshes was proposed by Nicolaidis (1993).

Recently, there seems to be increasing interest in action research about different Cartesian grid approaches. Those approaches have competitive advantages over the conventional body-fitted approach in simulating flows with moving boundaries, complicated shapes, or topological changes. Details about Cartesian grid approaches see Shyy et al. (1996), Udaykumar et al. (1996), Ye et al. (1999), and Mariani and Prata (2008).

Some recent works in engineering applications used meshless methods. One popular method is the meshless local Petrov-Galerkin (MLPG) successfully used by Lin and Atluri (2001), and Ahrem et al. (2006). Arefmanesh et al. (2008) applied a MLPG for the solution of the Navier-Stokes equations for the non-isothermal lid-driven cavity flow and other problems. Tsai et al. (2002) developed a meshless boundary elements method to solve 3D Stokes flows. The iterative process used in that study is similar to the process employed in Nicolás and Bermúdez (2007), the only difference is that these use a truly fixed point one,

---

<sup>1</sup>Department of Mechanical Engineering, Pontifical Catholic University of Parana, Rua Imaculada Conceição, 1155, Prado Velho, 80215-901, Curitiba, PR, Brazil.

<sup>2</sup>National Service of Commercial Learning, Center of Professional Education of Itajai, Rua Hercílio Luz, 293, 81301-001, Itajaí, SC, Brazil.

<sup>3</sup>Department of Computer Science and Statistics, Federal University of Santa Catarina, Bairro Trindade, 88040-900, Florianópolis, SC, Brazil.

with a different discretization time, while Nicolás and Bermúdez (2004) studied 2D flows.

Another method is Multiquadric Collocation Method (MCM) using radial basis function that has been used in a variety of works. For example, Ding et al. (2006) used MCM to solve the three-dimensional lid-driven cavity flow problem. Young et al. (2004) solved the Stokes flow problem in cavity by MCM. Chantasiriwan (2006) reports driven cavity results for the low Reynolds numbers  $Re = 0$ , which turns out to be a Stokes flow because of its infinity viscosity, and  $Re = 100$  using a MCM. Mai-Duy and Tran-Cong (2004) with the primitive variables formulation, report also the lid-driven cavity flow for  $Re = 100$  and  $Re = 0$ . Grimaldi et al. (2006) using a parallel multi-block method reported results for 2D and 3D lid-driven cavity problem. In Orsini et al. (2008) was presented a modified control volume method using a radial basis function interpolation to improve the prediction of the flux accuracy at the faces of the control volumes. The proposed approach validated a series de 1D and 3D test cases. Some efforts have been devoted recently in the development of works about finite-volume approach for unstructured meshes. See, for example, Eymard and Herbin (2003) and Blanc et al. (2005) for the solution the Stokes problem, Eymard and Herbin (2005) and Gallouët et al. (2000) for Navier-Stokes equations using staggered meshes, and Serrano et al. (2005) for the solution of Euler's equations. Meanwhile, Mathur and Murthy (1997a, 1997b) proposed a collocated SIMPLE-based solver avoiding spurious oscillations on pressure modes. Chénier et al. (2006) presented an original collocated finite-volume scheme to solve the Navier-Stokes equations in incompressible flows on structured or unstructured grids.

Among the unstructured meshes can be cited the meshes generated by Voronoi Diagrams (VD), which are independent of any global property, where elements and points can be added and deleted locally according to the flow features (Taniguchi and Kobayashi, 1991; Taniguchi et al., 1991).

In this work we develop a new finite-volume scheme to solve the Navier-Stokes equations for

the incompressible flows on collocated Voronoi meshes. For validation of this approach the square lid-driven cavity flow (Ghia et al., 1982; Vanka, 1986; Botella and Peyret, 1998; Bruneau and Saad, 2006; Grimaldi et al., 2006; Chantasiriwan, 2006; Nicolás and Bermúdez, 2007) is considered, because is a classical benchmark problem for the assessment of numerical methods and the validation of Navier-Stokes codes as can be seen in other research works.

The discretization of the Navier-Stokes and continuity equations is made using a linearization of first order, analogous to Newton's method. So, the main contribution of the present investigation is to report an accurate and efficient approach for solving Navier-Stokes equations using unstructured Voronoi meshes. In this regard, the present contribution adds to the effort that has been devoted in developing methods for unstructured meshes as the presented in Eymard and Erbin (2003) and Chénier et al. (2006). Such method employs unstructured grids and affords simplicity, yielding economic solvers of flow fields in complex geometries. Results for the lid-driven cavities employing the proposed approach are explored for different Reynolds numbers with emphasis being placed on the streamlines of the flow field, the centerline velocities profiles and pressure contours.

The rest of this article is organized as follows. In Section 2 is presented the main characteristics of the unstructured Voronoi mesh used in this work. In Section 3 and 4 is detailed the numerical approach proposed here. The results presented in this article in Section 5 refer essentially to the lid-driven cavity flow at Reynolds numbers in the range between 100 and 5,000 for comparison and validation with results in literature.

## 2 Voronoi Diagram

Dirichlet (1850) and Voronoi (1908) proposed a method whereby a given domain could be systematically decomposed into a set of packed convex polygons. A more formal definition can be stated. If a set of points is denoted by  $\{p_i\}$  then

the Voronoi region  $\{V_i\}$  can be defined as,

$$V_i = \{p \in \mathfrak{R}^2; d(p, p_i) < d(p, p_j), \forall j \neq i\}, \quad (1)$$

i.e., the Voronoi region  $\{V_i\}$  is the set of all points of  $p$  that are closer to  $p_i$  than to any other point, where  $d(p, p_i)$  is the Euclidean distance between  $p$  and  $p_i$ . The sum of all points  $p$  forms a Voronoi polygon that is given in Fig. 1. In two dimensions, the territorial boundary which forms a side of a Voronoi polygon must be midway between the two points which it separates, and is thus a segment of the perpendicular bisector of the line joining these two points. If the points, which have some segment of boundary in common, are joined by straight lines, the result is a Delaunay triangulation within the convex hull of the set of points  $\{p_i\}$ .

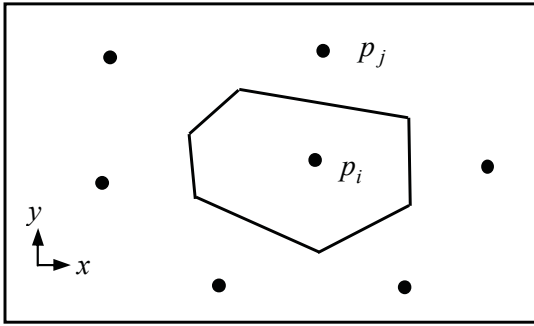


Figure 1: Voronoi polygon.

A common boundary between two Voronoi regions,  $V_i$  and  $V_j$ , is called Voronoi edge. Any Voronoi edge is a connected subset of a bisector  $B_{ij}$  of two points,  $p_i$  and  $p_j \in S$ , where  $S$  is a set of  $n$  points in the Euclidean plane. The following properties are consequence of the Voronoi Diagram shown in Fig. 2.

- (i) The straight line that joins point  $i$  to its neighbor  $j$  is always orthogonal the common edge to these points, for example,  $\overline{ij}$  is perpendicular to  $\overline{ae}$  for  $j = 5$ .
- (ii) The common edge to point  $i$  and its neighbor  $j$ , or its prolongation, is on the perpendicular bisector of the straight line that joins these points. For example, the straight line

$\overline{de}$  passes in the average point of the straight line  $d_{i4}$ , i.e., each point in the face is equidistant of exactly two points.

- (iii) Any Voronoi point  $v$  is the circumcenter of three points  $p_i, p_j$ , and  $p_k \in S$ . For example, the vertex  $d$  is the center of the circle that passes for points  $i, j = 3$  and  $j = 4$ , each vertex is equidistant of at least three points.
- (iv) Any Voronoi polygon is convex and especially connected, thus, the Voronoi diagram partitions the plane into a two-dimensional convex net.
- (v) The Voronoi polygons form a complete and disjoint partition of the Euclidean plane  $\mathfrak{R}^2$ .

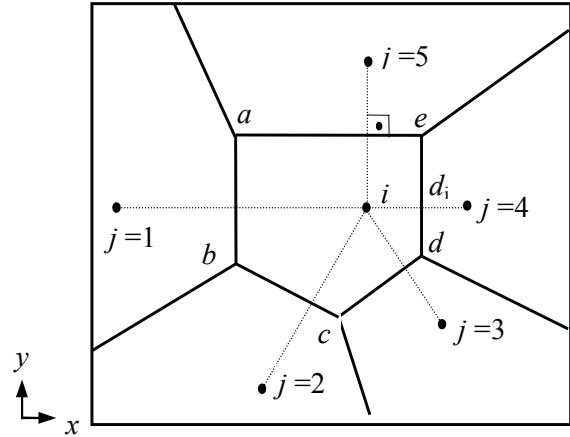


Figure 2: Voronoi Diagram formed by six convex polygons.

### 3 Numerical Method

The conservation equations, governing the transport of mass and momentum (Navier-Stokes equations) can be written in its vectorial two-dimensional laminar and unsteady form as,

$$\frac{\partial(\rho\phi)}{\partial t} + \vec{\nabla} \cdot \vec{J} = S^\phi \quad (2)$$

where  $\phi$  is any quantity vectorial or scalar (for example, velocity or pressure),  $\rho$  is the fluid density,  $\vec{J} = \rho\vec{V}\phi - \Gamma^\phi\vec{\nabla}\phi$  is the total flux of generic variable  $\phi$ ,  $\vec{V} = u\hat{i} + v\hat{j}$  is velocity vector where  $u$  and

$v$  are the velocity components in  $x$  and  $y$  directions, respectively,  $\Gamma$  is the diffusion coefficient,  $S$  is the source term, and  $\vec{\nabla} = \hat{i}\partial/\partial x + \hat{j}\partial/\partial y$  is the operator gradient.

In Tab. 1 are showed the correspondent terms for the different equations represented by Eq. (2).

Table 1: Terms in the transport equations.

Equations	$\phi$	$S^\phi$	$\Gamma^\phi$
Continuity	1	0	0
$x$ - momentum	$u$	$-\partial p/\partial x$	$\mu$
$y$ - momentum	$v$	$-\partial p/\partial y$	$\mu$

The system of equations, represented by continuity and Navier-Stokes equations, is discretized in space and time using the basic concepts of the finite volume method proposed in Patankar (1980). The discrete values of the pressure and velocities are located at the center of each cell as shown in Fig. 2 for a typical control volume.

The differential equations are then integrated over each volume yielding a set of algebraic equations for each variable. Thus the integration of the Eq. (2) for the generic variable  $\phi$  in each control volume is given by

$$\iiint_{t,V} \frac{\partial(\rho\phi)}{\partial t} dt dV + \iiint_{V,t} (\vec{\nabla} \cdot \vec{J}) dV dt = \iiint_{V,t} S^\phi dV dt. \quad (3)$$

We now proceed to discretize each of the terms in Eq. (3) for the control volume shown in Fig. 2, for example, thus the first term can be expressed as,

$$\iiint_{t,V} \frac{\partial(\rho\phi)}{\partial t} dt dV = Ap_i^0 (\phi_i - \phi_i^0) \quad (4)$$

where  $Ap_i^0 = \rho_i \Delta V_i / \Delta t$  is the coefficient in the nodal point  $i$ ,  $\Delta t$  is the time step size,  $\Delta V_i$  is the volume of the irregular control volume, i.e., the volume of the convex polygon generated by Voronoi Diagram,  $\phi_i^0$  is the generic variable  $\phi$  valued in the previous time, and  $\phi_i$  is the generic variable  $\phi$  valued in the actual time.

The second term, the liquid flow  $\vec{J}$  normal through each cell face of the control volume, is evaluated using the divergence theorem as,

$$\iiint_{V,t} (\vec{\nabla} \cdot \vec{J}) dV dt = \iint_{S_n} (\vec{J} \cdot \hat{n}) dS = \sum_{j=1}^{N(i)} J_{ij} S_{ij} \quad (5)$$

where  $S_n$  is the control-surface,  $\hat{n}$  is a unit vector normal to the control-surface,  $J_{ij}$  is the normal component of flux  $\vec{J}$  in each cell face of the control volume, as shown in Fig. 2,  $S_{ij}$  is the cell face between the points  $i$  and  $j$ , where  $j$  is the index of neighbor of  $i$ ,  $N(i)$  is the number of neighbors of the nodal point  $i$ , and  $J_{ij} S_{ij}$  is the liquid flow that cross the face  $ij$ .

Considering  $W_{ij}$  as the normal component of velocity evaluated on the face  $ij$ , that is responsible by advection of  $\phi$  through of the face  $ij$ , and  $n$  as the normal direction in each face  $ij$  (auxiliary co-ordinate) then  $J_{ij}$  (see Eq. (5)) is calculated as,

$$J_{ij} = \left[ \rho W \phi - \Gamma^\phi \frac{\partial \phi}{\partial n} \right]_{ij} = \rho_{ij} W_{ij} \phi_{ij} - \Gamma_{ij}^\phi \left( \frac{\partial \phi}{\partial n} \right)_{ij} \quad (6)$$

where the variables with index  $ij$  are evaluated on the face  $ij$  through adequate averages to each case as presented in Patankar (1980), for example, the density,  $\rho_{ij}$ , is obtained through of the arithmetic mean as,  $\rho_{ij} = (\rho_i + \rho_j)/2$ , while the diffusion coefficient,  $\Gamma_{ij}^\phi$ , is evaluated through of the harmonic mean as,  $\Gamma_{ij}^\phi = 2\Gamma_i^\phi \Gamma_j^\phi / (\Gamma_i^\phi + \Gamma_j^\phi)$ , and  $\left. \frac{\partial \phi}{\partial n} \right|_{ij} = (\phi_i - \phi_j)/L_{ij}$  is approached by central difference of first order, where  $L_{ij}$  is the Euclidean distance between the points  $i$  and  $j$ . The evaluation of  $W_{ij}$ , in the present work, is made through of the simple arithmetic mean between the projected normal components in the direction  $ij$  given by

$$W_{ij} = \frac{(w_i)_{ij} + (w_j)_{ij}}{2} \quad (7)$$

where  $(w_i)_{ij} = u_i e_{x_{ij}} + v_i e_{y_{ij}}$  and  $(w_j)_{ij} = u_j e_{x_{ij}} + v_j e_{y_{ij}}$  are the normal components to face  $ij$  evaluated on the nodal points  $i$  and  $j$ , as shown in Fig. 3.

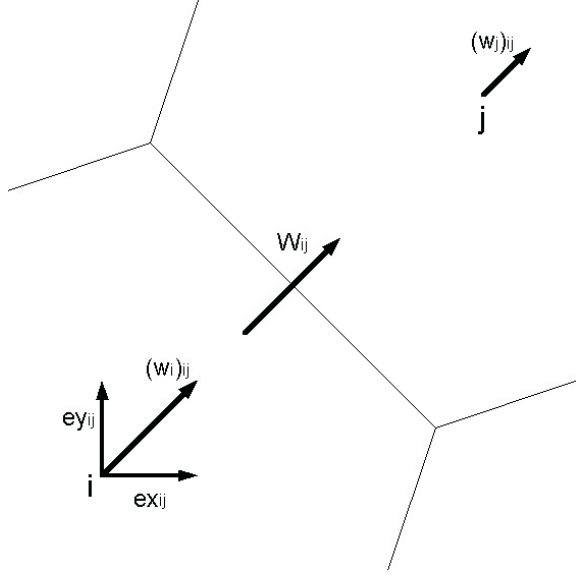


Figure 3: Normal components to the face  $ij$  on nodal points  $i$  and  $j$ .

The Eq. (7) can be rewritten as,

$$W_{ij} = u_{ij}ex_{ij} + v_{ij}ey_{ij} \quad (8)$$

where  $u_{ij}$  and  $v_{ij}$  are, respectively, the horizontal and vertical components of velocity  $\vec{V}$  evaluated on the face  $ij$  of control volume.

Lastly, to the third term we proceed to discretize using the mean as,

$$\iiint_{V,t} S^\phi dV dt = \bar{S}_i^\phi \Delta V_i, \quad (9)$$

where  $\bar{S}_i^\phi$  is the mean value of  $S^\phi$  in the control volume  $i$ .

The Eq. (3) can be rewritten as an algebraic equation of the form,

$$Ap_i^0(\phi_i - \phi_i^0) + \sum_{j=1}^{N(i)} \left[ \rho W \phi - \Gamma^\phi \frac{\partial \phi}{\partial z} \right]_{ij} S_{ij} = \bar{S}_i^\phi \Delta V_i. \quad (10)$$

To solve the Eq. (10) appears a coupled system of nonlinear equations which requires the solution of a sparse and not banded matrix, especially if the mesh was randomly generated. The main difficulties related to the numerical solution of Eq.

(10) are the unknown pressure and the advection term. The nonlinear advective term  $\rho W \phi$  needs a linearization process, thus the system of nonlinear equations can be transformed in a system of linear equations and solved through an iterative method. Among the many available versions for linearization process we choose a simple which is of first-order accurate. The low-order accuracy is compensated by easy implementation, less cost in computational time, good stability, and robustness properties.

The present work has for objective to evaluate the linearization proposed that use the Newton's method. This kind of linearization was chosen because it produces quadratic convergent approximations in conformity with Burden and Faires (1985). In this method, a system of nonlinear equations is solved through of a sequence of linear systems. To follow it is presented the discretization for generic variable  $\phi$  using the linearization proposed.

#### 4 Linearization by Newton's Method

Let us modify the advective term presented in the Eq. (10) substituting  $\phi_{ij} = u_{ij}$ , such as,

$$G(u_{ij}, v_{ij}) = \rho_{ij} W_{ij} u_{ij}. \quad (11)$$

Substituting the Eq. (8) in Eq. (11) the advective term follows,

$$G(u_{ij}, v_{ij}) = \rho_{ij}(u_{ij}ex_{ij} + v_{ij}ey_{ij})u_{ij}. \quad (12)$$

The term  $G(u_{ij}, v_{ij})$  can be linearized by Newton's method as,

$$G(u_{ij}, v_{ij}) \cong G(u_{ij}^*, v_{ij}^*) + \frac{\partial G}{\partial u_{ij}} \Big|_{u_{ij}^*, v_{ij}^*} (u_{ij} - u_{ij}^*) + \frac{\partial G}{\partial v_{ij}} \Big|_{u_{ij}^*, v_{ij}^*} (v_{ij} - v_{ij}^*) + \dots \quad (13)$$

Differencing the Eq. (12) with respect to  $u_{ij}$  and  $v_{ij}$ , after replacing  $(u_{ij}, v_{ij})$  by  $(u_{ij}^*, v_{ij}^*)$ , such procedure follows,

$$\begin{aligned} \frac{\partial G}{\partial u_{ij}} \Big|_{u_{ij}^*, v_{ij}^*} &= \rho_{ij}(u_{ij}^*ex_{ij} + v_{ij}^*ey_{ij}) + \rho_{ij}ex_{ij}u_{ij}^* \\ &= \rho_{ij}W_{ij}^* + \rho_{ij}ex_{ij}u_{ij}^* \end{aligned} \quad (14)$$

$$\left. \frac{\partial G}{\partial v_{ij}} \right|_{u_{ij}^*, v_{ij}^*} = \rho_{ij} e y_{ij} u_{ij}^* \quad (15)$$

where \* denote the estimated values in the previous iteration.

Substituting Eqs. (12), (14) and (15) in Eq. (13) after of some algebraic manipulations such equation can be written in the following form,

$$G(u_{ij}, v_{ij}) = \rho_{ij} W_{ij}^* u_{ij}^* + (\rho_{ij} W_{ij}^* + \rho_{ij} e x_{ij} u_{ij}^*) (u_{ij} - u_{ij}^*) + (\rho_{ij} e y_{ij} u_{ij}^*) (v_{ij} - v_{ij}^*) \quad (16)$$

Then, the complete equation of the diffusive and convective fluxes, the Eq. (6), for  $\phi_{ij} = u_{ij}$ , for example, has the form,

$$J_{ij} = \left( \rho_{ij} W_{ij} u_{ij} - \mu_{ij} \left. \frac{\partial u}{\partial n} \right|_{ij} \right) = \left( G(u_{ij}, v_{ij}) - \mu_{ij} \left. \frac{\partial u}{\partial n} \right|_{ij} \right) \quad (17)$$

Substituting the Eqs. (8) and (16) in Eq. (17), we obtain

$$J_{ij} = \rho_{ij} \left\{ u_{ij}^* [e x_{ij} (u_{ij} - u_{ij}^*) + e y_{ij} (v_{ij} - v_{ij}^*)] + v_{ij}^* e y_{ij} u_{ij} \right\} - \mu_{ij} \left( \frac{u_j - u_i}{L_{ij}} \right). \quad (18)$$

A similar development is adopted for the linearization of the equation for  $v$  velocity, which will be omitted in this manuscript, such linearization results in

$$J_{ij} = \rho_{ij} \left\{ v_{ij}^* [e x_{ij} (u_{ij} - u_{ij}^*) + e y_{ij} (2v_{ij} - v_{ij}^*)] + u_{ij}^* e x_{ij} v_{ij} \right\} - \mu_{ij} \left( \frac{v_j - v_i}{L_{ij}} \right). \quad (19)$$

In Eqs. (18) and (19) to evaluate the velocities,  $u$  and  $v$ , in the interface  $ij$ , is used the following well known first-order interpolation, Upwind Differencing Scheme (UDS), where  $u_{ij} = u_i \delta_{ij}^+ + u_j \delta_{ij}^-$  and  $v_{ij} = v_i \delta_{ij}^+ + v_j \delta_{ij}^-$  with  $\delta_{ij}^+ = \max(0, F_{ij}) / |F_{ij}|$  and  $\delta_{ij}^- = \max(0, -F_{ij}) / |F_{ij}|$ , where  $F_{ij} = \rho_{ij} W_{ij} S_{ij}$  is convective flux that cross each interface  $ij$ .

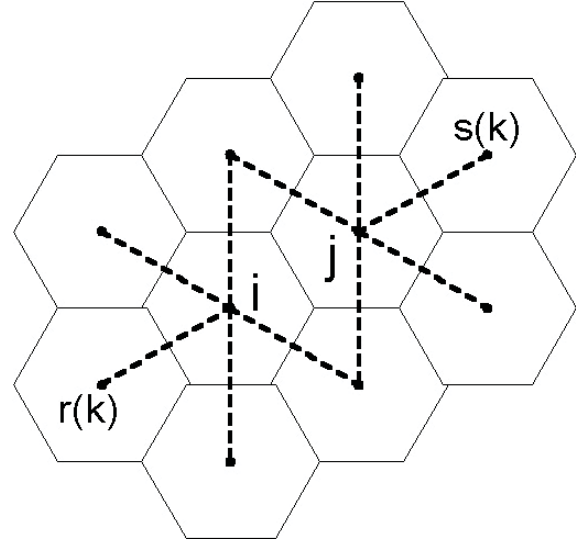


Figure 4: Neighbors  $i$  and  $j$  and its respective neighborhoods  $r(k)$  and  $s(k)$ .

The subscript  $j$  used until here as the neighbors of the control volume  $i$  will be substituted by  $k$  or  $r(k)$  when concerns to control volume  $i$  and by  $k$  or  $s(k)$  if refers to control volume  $j$ , as shown in Fig. 4.

Lastly, substituting the Eq. (18) in Eq. (10) for  $\phi = u$ , and subtracting the discretized continuity equation,  $\sum_{k=1}^{N(i)} F_{ik} = 0$ , multiplied by  $u_i$  on left equation we obtain,

$$A p_i^u u_i = \sum_{k=1}^{N(i)} A_{ik}^u u_{r(k)} + b_i^u \quad (20)$$

where

$$b_i^u = \Omega_{ik}^u(i) + A p_i^0 u_i^0,$$

$$\Omega_{ik}^u(i) = -(\nabla P)_i^x \Delta V_i + \sum_{k=1}^{N(i)} \alpha_{ik}^u u_{ik}^*,$$

$$A p_i^u = A p_i^0 + \sum_{k=1}^{N(i)} A_{ik}^u - \alpha_{ik}^u, \quad (21)$$

$$D_{ik}^u = \mu_{ik} \left( \frac{S_{ik}}{L_{ik}} \right),$$

$$F_{ik} = \rho_{ik} W_{ik}^* S_{ik},$$

$$A_{ik}^u = -(\alpha_{ik}^u + F_{ik}) \delta_{ik} - D_{ik},$$

where  $b_i$  is the source term of control volume  $i$ ,  $u_i^0$  is the velocity in the previous time,  $u_{ik}^*$ ,  $v_{ik}^*$  and  $W_{ik}^*$  are evaluated in the interface  $ik$ ,  $\alpha_{ik}^u = \rho_{ik} u_{ik}^* ex_{ik} S_{ik}$ ,  $A_{pi}$  is the central coefficient of the control volume  $i$ , and  $A_{ik}$  are neighbors coefficients of the control volume  $i$ . The discretized equation for velocity  $v$  can be obtained adopting a development similar to velocity  $u$ .

Until here the governing equations for the velocities were obtained, however is to need evaluated the pressure used in those equations. For the coupling between pressure and velocities, the SIMPLE algorithm (Semi Implicit Method for Pressure Linked Equations) was employed (Patankar, 1980). The pressure gradient in Eq. (20) is evaluated as,

$$\nabla P_x = \frac{\sum_{j=1}^{NV} (\vec{\nabla} p_{ij} \cdot \hat{i}) g_{ij}}{\sum_{j=1}^{NV} g_{ij} |ex_{ij}|} \quad (22)$$

where  $g_{ij} = S_{ij}/L_{ij}$  and  $\vec{\nabla} p_{ij} = \left( \frac{p_i - p_j}{L_{ij}} \right) \cdot (ex_{ij} \hat{i} + ey_{ij} \hat{j})$ .

## 5 Results and Discussion

In this section, we compare the previous scheme on steady solutions in two-dimensional lid driven cavity flow for which a vast specialized literature is available. The first results were given by Ghia et al. (1982) and Schreiber and Keller (1983) who reported accurate solutions to the steady flow solution over a range of Reynolds numbers,  $Re = UL/\nu$ , where  $U$  is the constant lid velocity,  $L$  is the cavity dimension, and  $\nu$  is the kinematic viscosity of the fluid, and since then, many authors (Vanka, 1986; Botella and Peyret, 1998; Bruneau and Saad, 2006; Grimaldi et al., 2006; Chantasiriwan, 2006; Nicolás and Bermúdez, 2007) compared their results to those works.

A cavity, similar to studied by Ghia et al. (1982), is shown in Fig. 5a. In the same figure are shown two kinds of Voronoi meshes used in this work, the first kind is the mesh formed by 530 random control volumes while the second kind is the mesh formed by 6,400 ( $80 \times 80$ ) hexagonal control vol-

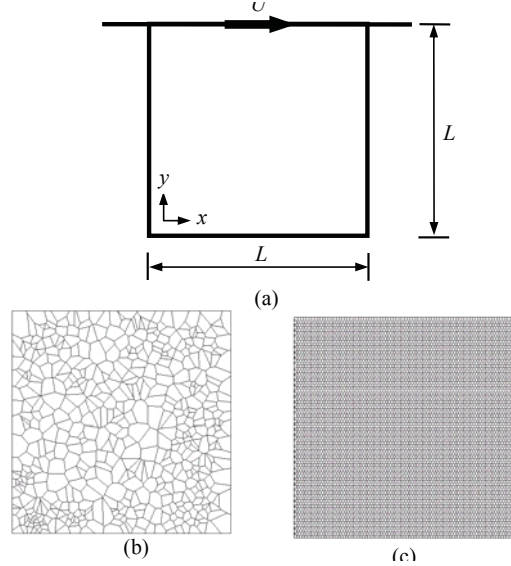


Figure 5: (a) Lid driven cavity and computational mesh formed by (b) 530 and (c)  $80 \times 80$  control volumes.

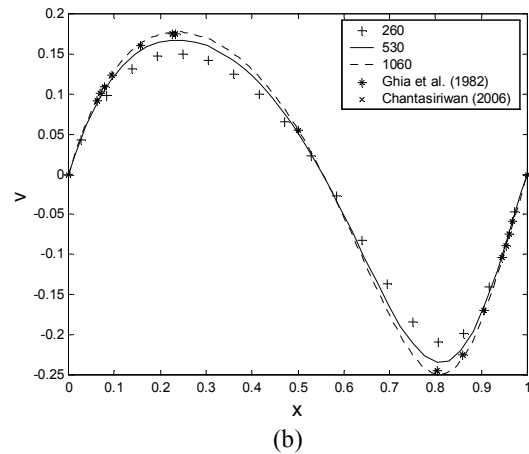
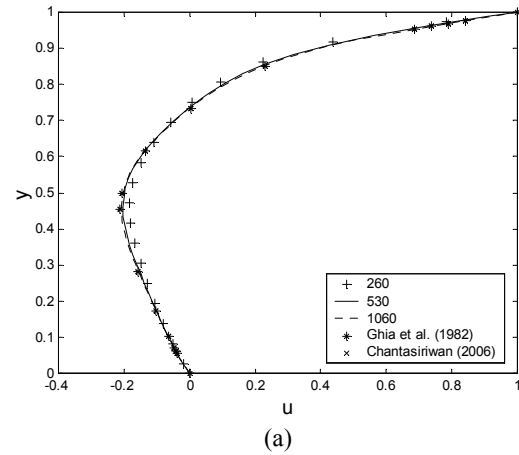


Figure 6: Profiles of (a)  $u$ -velocity along vertical centerline and (b)  $v$ -velocity along horizontal centerline cavity for  $Re = 100$ .

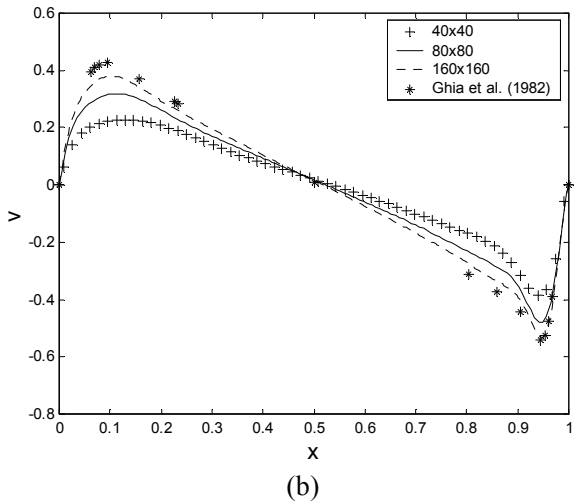
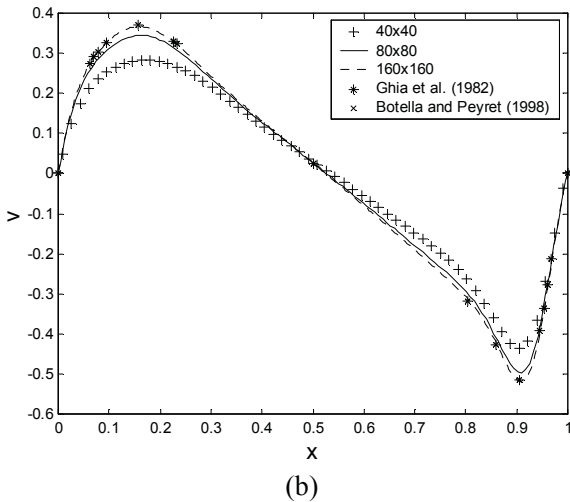
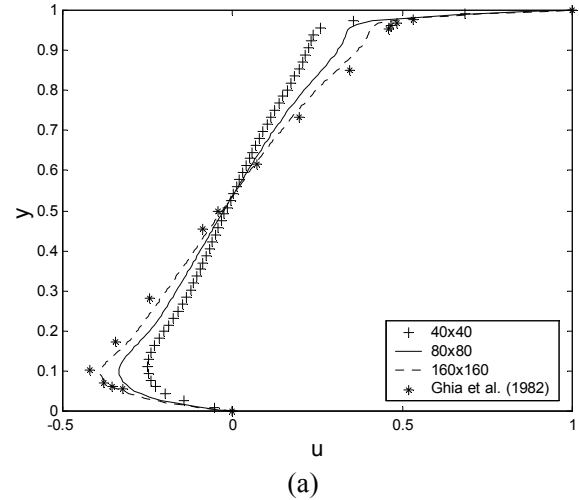
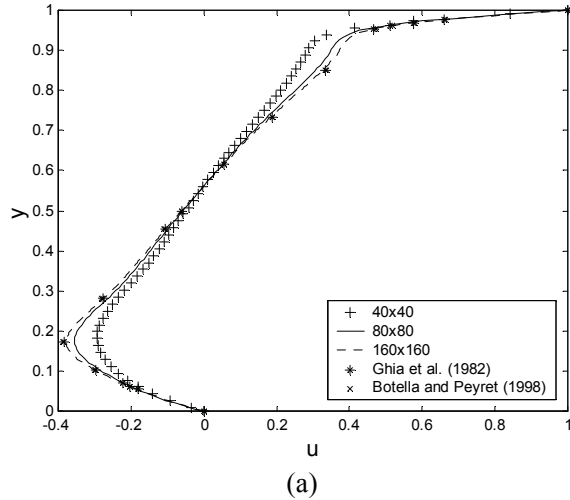


Figure 7: Profiles of (a)  $u$ -velocity along vertical centerline and (b)  $v$ -velocity along horizontal centerline cavity at  $Re = 1,000$ .

Figure 8: Profiles of (a)  $u$ -velocity along vertical centerline and (b)  $v$ -velocity along horizontal centerline cavity at  $Re = 3,200$ .

umes, as showed in the Fig. 5b, meanwhile, were used other Voronoi meshes.

The boundary conditions for the two-dimensional lid-driven cavity presented in Fig. 5 are given as follows,

$$\begin{aligned}
 u &= U, v = 0 \text{ at } y = L \text{ and } 0 \leq x \leq L, \\
 u &= 0, v = 0 \text{ at } y = 0 \text{ and } 0 \leq x \leq L, \\
 u &= 0, v = 0 \text{ at } x = 0 \text{ and } 0 < y < L, \\
 u &= 0, v = 0 \text{ at } x = L \text{ and } 0 < y < L.
 \end{aligned} \tag{23}$$

The solution to the system of linear equations generated from discretization was obtained through

of a stabilized conjugate gradient squared method with incomplete Cholesky preconditioning, see details in Ferziger and Peric (1997). Computations have been performed on a computer IBM 9076 SP/2 because the software was previously developed in IBM AIX system. An under-relaxation parameter of 0.5 was used in order to obtain a stable convergence for the solution of momentum equation while 0.5 was used in the solution of pressure equation.

We use the solver for the two kinds of unstructured meshes. The hexagonal meshes formed by  $40 \times 40$ ,  $80 \times 80$  and  $160 \times 160$  control volumes,

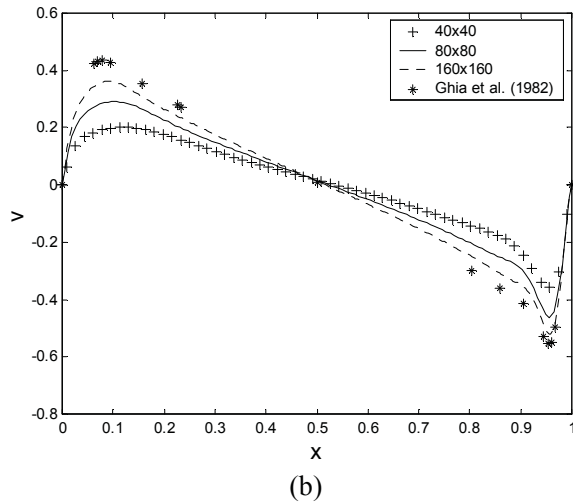
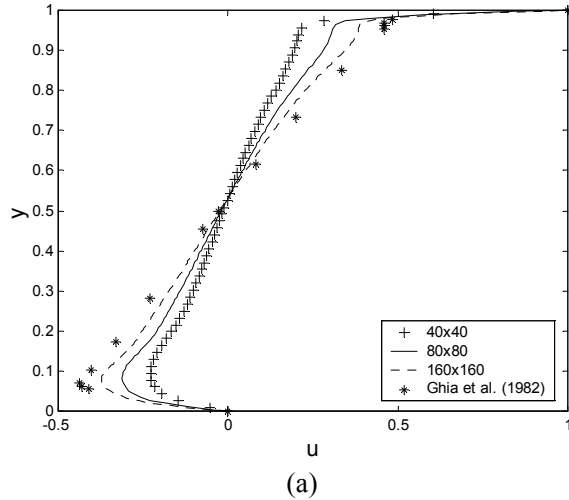


Figure 9: Profiles of (a)  $u$ -velocity along vertical centerline and (b)  $v$ -velocity along horizontal centerline cavity at  $Re = 5,000$ .

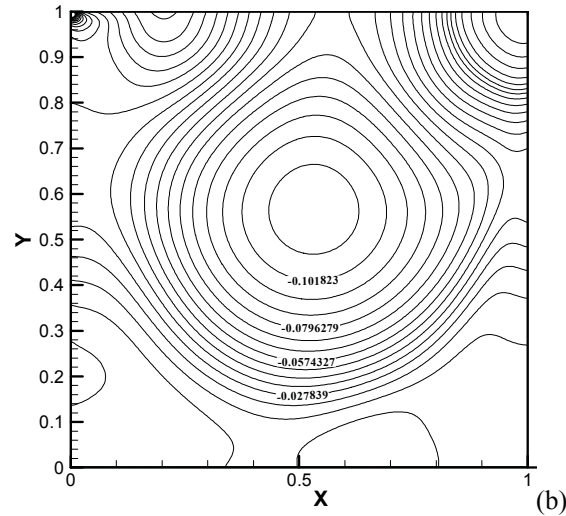
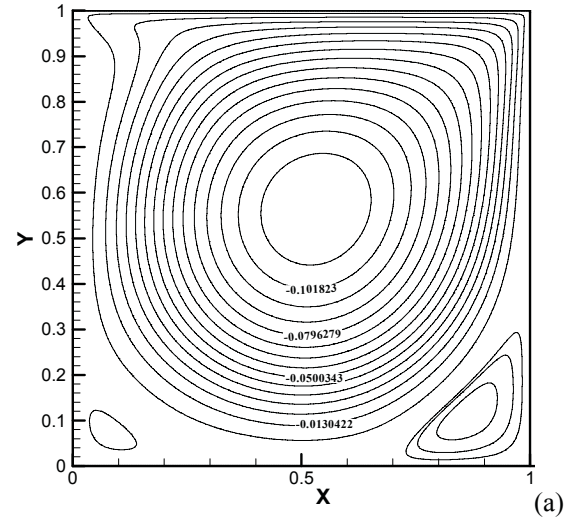


Figure 10: Solution at  $Re = 1,000$  computed with present scheme on grid  $160 \times 160$ , (a) stream-function and (b) pressure fields.

and also random meshes with 260, 530 and 1060 control volumes. Simulation results were collected with Reynolds numbers from 100 until 5,000. As convergence criterion the desired precision,  $\sum_{j=1}^{N(i)} |F_{ij}^k| \leq 10^{-8}$ , was used.

Figure 6 shows  $u$  and  $v$  velocities profiles for Reynolds number equals 100 along the vertical centerline ( $x = L/2$ ) and horizontal centerline ( $y = L/2$ ) for the velocities in directions  $x$  and  $y$ , respectively, using the random meshes with 260, 530 and 1060 control volumes. Note that the results obtained with the mesh formed by 1060 control

volumes are in agreement with Ghia et al. (1982) and Chantasiriwan (2006).

Figures 7 to 9 present  $u$  and  $v$  velocities profiles for Reynolds  $Re = 1,000$ ,  $Re = 3,200$  and  $Re = 5,000$  along the vertical centerline ( $x = L/2$ ) and horizontal centerline ( $y = L/2$ ) for the velocities in directions  $x$  and  $y$ , respectively. Included in those figures are the available results of Ghia et al. (1982). For  $Re = 1,000$ , all results agree well with Ghia et al. (1982), Botella and Peyret (1998), and Grimaldi et al. (2006), meanwhile the results of the last author are not presented in Fig. 7 because are equal to of other authors. The re-

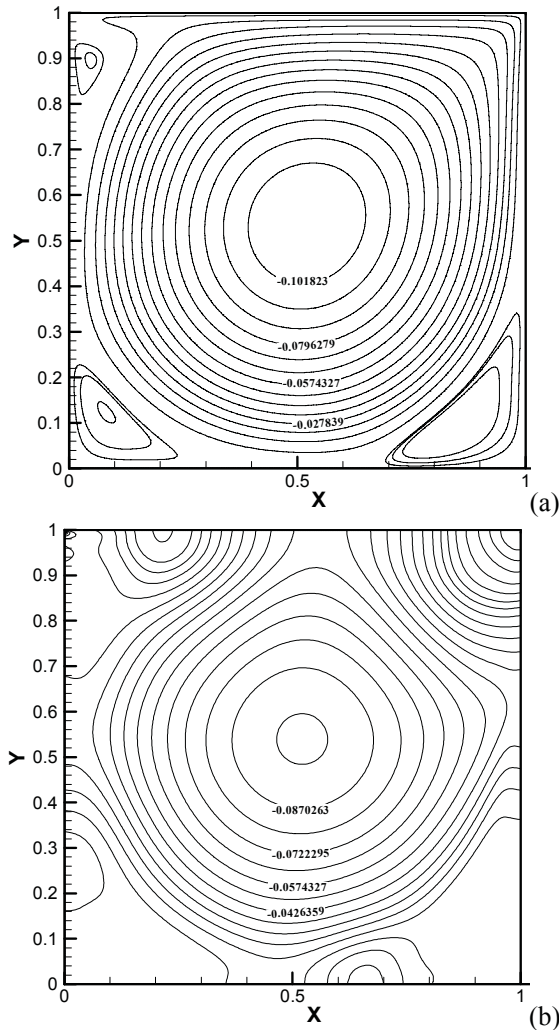


Figure 11: Solution at  $Re = 3,200$  computed with present scheme on grid  $160 \times 160$ , (a) stream-function and (b) pressure fields.

sults indicate that for  $Re = 1,000$  the mesh formed by  $160 \times 160$  control volumes employed was adequate. As Reynolds increases, however, the inadequacy of coarse meshes gradually becomes apparent, as already observed by Ghia *et al.* (1982), see Figs. 8 and 9.

We compare our results at  $Re = 1,000$  to those of the literature (Ghia *et al.*, 1982; Vanka, 1986; Botella and Peyret, 1998; Bruneau and Saad, 2006) and the data are presented in Tab. 2. We can see that the present results, with the grid formed by  $160 \times 160$  control volumes, are in agreement with the literature.

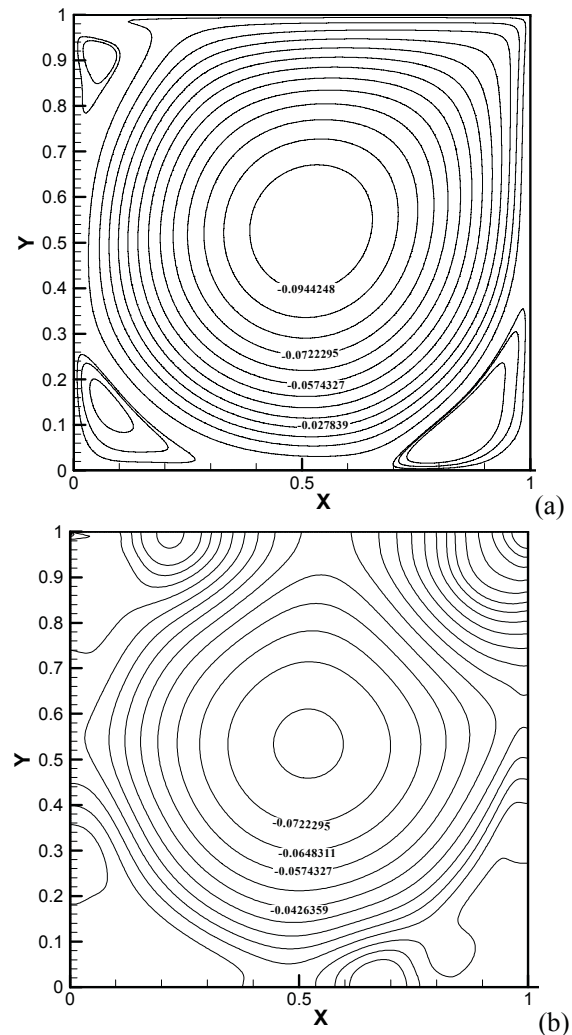


Figure 12: Solution at  $Re = 5,000$  computed with present scheme on grid  $160 \times 160$ , (a) stream-function and (b) pressure fields.

For Reynolds number  $Re = 5,000$  there are some comparisons available in the literature meanwhile there is no very accurate results as in the previous studied case. We choose our results obtained with the same grid  $160 \times 160$  control volumes. The comparison for  $Re = 5000$  with the results of the literature is shown in Table 3. Nevertheless our results are consistent with results found by Ghia *et al.* (1982), Vanka (1986), and Bruneau and Saad (2006).

Other solution computed with our method is plotted in Figs. 10 to 12, where are showed stream functions and pressure fields. Figure 10a shows

Table 2: Comparison of various works on the primary and secondary vortex at  $Re = 1,000$ .

Authors	Grid	$\psi_{\max}$	$\omega$	$X$	$Y$
Present	$160^2$	0.1175	2.0475	0.47	0.56
Ghia et al.	$128^2$	0.1179	2.0497	0.47	0.56
Schreiber	$140^2$	0.1160	2.0497	0.47	0.56
Botella & Peyret	160	0.1189	2.0678	0.47	0.57
Bruneau & Saad	$128^2$	0.1179	2.0508	0.47	0.56
		$\psi_{\min}$			
Present	$160^2$	$-1.75 \times 10^{-3}$	-1.135	0.14	0.11
Ghia et al.	$128^2$	$-1.75 \times 10^{-3}$	-1.155	0.14	0.11
Schreiber	$140^2$	$-1.70 \times 10^{-3}$	-0.999	0.14	0.11
Botella & Peyret	160	$-1.73 \times 10^{-3}$	-1.112	0.14	0.11
Bruneau & Saad	$128^2$	$-1.70 \times 10^{-3}$	-1.130	0.14	0.11

Table 3: Comparison of various works on the primary and secondary vortex at  $Re = 5,000$ .

Authors	Grid	$\psi_{\max}$	$\omega$	$X$	$Y$
Present	$160^2$	0.1174	1.831	0.48	0.53
Ghia et al.	$256^2$	0.1190	1.860	0.49	0.54
Vanka	$160^2$	0.0920	—	0.49	0.53
Bruneau & Saad	$256^2$	0.1206	1.913	0.48	0.54
		$\psi_{\min}$			
Present	$160^2$	$-2.95 \times 10^{-3}$	-2.560	0.19	0.06
Ghia et al.	$256^2$	$-3.08 \times 10^{-3}$	-2.664	0.19	0.07
Vanka	$160^2$	$-5.49 \times 10^{-3}$	—	0.15	0.08
Bruneau & Saad	$256^2$	$-3.04 \times 10^{-3}$	-2.633	0.19	0.07

a large primary vortex with two secondary vortices in the two bottom corners at  $Re = 1,000$ . The value 0.1175 of the stream function is chosen to represent the primary vortex core. The contours of pressure are plotted in Fig. 10b and are in agreement with results of Bruneau and Saad (2006).

Using Reynolds number  $Re = 3,200$  and  $Re = 5,000$  the solutions are plotted in Figs. 11 and 12. Those figures exhibit two secondary vortices in the bottom corners and a third vortex in the upper left corner and much stronger gradients than the solution at  $Re = 1000$  as observed by Ghia et al. (1982), Bruneau and Saad (2006), and Nicolás and Bermúdez (2007).

## 6 Conclusions

The present work proposed a scheme for linearization of advective terms found in the Navier-

Stokes equations. Those equations were solved in unstructured meshes formed by Voronoi Diagrams using finite volume method. Thus, based on the obtained simulation results, it was possible to conclude that the scheme proposed has good performance when compared with results of literature. The main advantage of the current methodology is that flows with extremely complex internal boundaries can be simulated with relative ease on unstructured meshes formed by Voronoi Diagram, some tests are being developed in this direction. The obtained results with the scheme proposed in this work were mainly compared with the results obtained by Ghia et al. (1982) showing a good agreement.

## References

Ahrem, R.; Beckert, A.; Wendland, H. (2006): A meshless spatial coupling scheme for large-scale fluid-structure interaction problems, *CMES*:

*Computer Modeling in Engineering & Sciences*, Vol 12, No. 2, pp. 121-136.

**Arefmanesh, A.; Najafi, M.; Abdi, H.** (2008): Meshless local Petrov-Galerkin method with unity test function for non-isothermal fluid flow, *CMES: Computer Modeling in Engineering & Sciences*, Vol. 25, No. 1, pp. 9-22.

**Blanc, P.; Eymard, R.; Herbin, R.** (2005): A staggered finite volume scheme on general meshes for the generalized Stokes problem in two space dimensions, *Int. J. Finite Volumes*, <http://averoes.math.univparis13.fr/JOURNAL/IJFV>.

**Botella, O.; Peyret, R.** (1998): Benchmark spectral results on the lid-driven cavity flow, *Computers & Fluids*, Vol. 27, No. 4, pp. 421-433.

**Bruneau, C.-H.; Saad, M.** (2006): The 2D lid-driven cavity problem revisited. *Computers & Fluids*, Vol. 35, No. 3, pp. 326-348.

**Burden, R. L.; Faires, J. D.** (1985): *Numerical analysis*, PWS, Boston, USA.

**Chantasiriwan, S.** (2006): Performance of multiquadric collocation method in solving lid-driven cavity flow problem with low Reynolds number, *CMES: Computer Modeling in Engineering & Sciences* Vol. 15, No. 3, pp. 137-146.

**Chénier, E.; Eymard, R.; Touazi, Q.** (2006): Numerical results using a collocated finite-volume scheme on unstructured grids for incompressible fluid flows, *Numer. Heat Transfer Part B*, Vol. 49, No. 3, pp. 259-276.

**Ding, H.; Shu, C.; Yeo, K. S.; Xu, D.** (2006): Numerical computation of three-dimensional incompressible viscous flows in the primitive variable form by local multiquadratic differential quadrature method, *Comp. Methods in Appl. Mech. Engr.*, Vol. 195, No. 7-8, pp. 516-533.

**Dirichlet, G. L.** (1850): Über die reduction der positiven quadratischen formen mit drei unbestimmten ganzen zahlen, *Z. Reine Angew. Math.*, Vol. 40, pp. 209-227.

**Eymard, R.; Herbin, R.** (2003): A cell-centered finite volume scheme on general meshes for the Stokes equations in two space dimensions, *Comptes Rendus Mathématique*, Vol. 337, No. 2,

pp. 125-128.

**Eymard, R.; Herbin, R.** (2005): A staggered finite volume scheme on general meshes for the Navier-Stokes equations in two space dimensions, *Int. J. Finite Volumes*, <http://averoes.math.univparis13.fr/JOURNAL/IJFV>.

**Ferziger, J. H.; Peric, M.** (1997): *Computational methods for fluid dynamics*. Springer Verlag, Berlin, Heidelberg, Germany.

**Gallouët, T.; Herbin, R.; Vignal, M. H.** (2000): Error estimates on the approximate finite volume solution of convection diffusion equations with general boundary conditions, *SIAM Journal on Numerical Analysis*, Vol. 37, No. 6, pp. 1935-1972.

**Ghia, U.; Ghia, K. N.; Shin, C. T.** (1982): High-resolution solutions for incompressible flow using the Navier-Stokes equations and multigrid method, *J. Comp. Phys.*, Vol. 48, pp. 387-411.

**Grimaldi, A.; Pascazio, G.; Napolitano, M.** (2006): A parallel multi-block method for the unsteady vorticity-velocity equations, *CMES: Computer Modeling in Engineering & Sciences*, Vol 14, No. 1, pp. 45-56.

**Harlow, F.; Welch, J.** (1965): Numerical calculation of time-dependent viscous incompressible flow of fluid with a free surface, *Phys. Fluids*, Vol. 8, No. 12, pp. 2182-2189.

**Li, R.; Chen, Z.; Wu, W.** (2000): *Generalized difference methods for differential equations: Numerical analysis of finite volume methods*, Marcel Dekker, New York, USA.

**Lin, H.; Atluri, S. N.** (2001): The meshless local Petrov-Galerkin (MLPG) method for solving incompressible Navier-Stokes equations, *CMES: Computer Modeling in Engineering & Sciences*, Vol. 2, No. 2, pp. 117-142.

**Mai-Duy, N.; Tran-Cong, T.** (2004): Boundary integral-based domain decomposition technique of Navier-Stokes equations. *CMES: Computer Modeling in Engineering & Sciences*, Vol. 6, No. 1, pp. 59-75.

**Mariani, V. C.; Prata, A. T.** (2008): A Eulerian-Lagrangian method applied to fluid flow in lid-driven cavities with irregular bottom walls. *Nu-*

mer. *Heat Transfer Part B*, Vol. 53, No. 3, pp. 1-28.

**Mathur, S. R.; Murthy, J. Y.** (1997): A pressure-based method for unstructured meshes, *Numer. Heat Transfer Part B*, Vol. 31, pp. 195–215.

**Mathur, S. R.; Murthy, J. Y.** (1997): Pressure boundary conditions for incompressible flow using unstructured meshes, *Numer. Heat Transfer Part B*, Vol. 32, pp. 283–298.

**Mishev, I.** (1998): Finite volume methods on Voronoi meshes, *Numer. Methods Partial Differential Equations*, Vol. 14, pp. 193–212.

**Nicolaides, R. A.** (1993): The covolume approach to computing incompressible flows, in M. D. Gunzburger and R. A. Nicolaides (eds.), *Incompressible Computational Fluid Dynamics*, Cambridge University Press, Cambridge, UK, pp. 295-333.

**Nicolás, A.; Bermúdez, B.** (2004): 2D Incompressible viscous flows at moderate and high Reynolds numbers. *CMES: Computer Modeling in Engineering & Sciences*, Vol. 6, No. 5, pp. 441-451.

**Nicolás A.; Bermúdez, B.** (2007): Viscous incompressible flows by the velocity-vorticity Navier-Stokes equations, *CMES: Computer Modeling in Engineering & Sciences*, Vol 20, No. 2, pp. 73-83.

**Orsini, P.; Power, H.; Morvan, H.** (2008): Improving volume element methods by meshless radial basis function techniques, *CMES: Computer Modeling in Engineering & Sciences*, Vol. 23, No. 3, pp. 187-207.

**Patankar, S. V.** (1980): *Numerical heat transfer and fluid flow*, Hemisphere Publishing Corporation, USA.

**Schreiber, R.; Keller, H. B.** (1983): Driven cavity flows by efficient numerical techniques, *J. Comp. Phys.*, Vol. 49, No. 2, pp. 310-333.

**Serrano, M.; Español, P.; Zúñiga, I.** (2005): Voronoi fluid particle model for Euler equations, *J. of Statistical Physics*, Vol. 121, No. 1-2, pp. 133-147.

**Shyy, W.; Udaykumar, H. S.; Rao, M. M.; Smith, R. W.** (1996): *Computational Fluid Dy-*

*namics with Moving Boundaries*, Taylor & Francis, UK.

**Taniguchi, N.; Arakawa, C.; Kobayashi, T.** (1991): Construction of a flow-simulating method with finite volume based on a Voronoi Diagram, *JSME International Journal, Serie II*, Vol. 34, No. 1, pp. 18-23.

**Taniguchi, N.; Kobayashi, T.** (1991): Finite volume method on the unstructured grid system, *Computers & Fluids*, Vol. 19, No. 3-4, pp. 287-295.

**Tsai, C., Young, D. L., Cheng A. H.** (2002): Meshless BEM for Three-Dimensional Stokes Flows. *CMES: Computer Modeling in Engineering & Sciences*, Vol. 3, No. 1, 117-128.

**Udaykumar, H. S.; Shyy, W.; Rao, M. M.** (1996): ELAFINT: A mixed Eulerian-Lagrangian method for fluid flows with complex and moving boundaries, *Int. J. Numerical Methods in Fluids*, Vol. 22, No. 8, pp. 691-712.

**Vanka, S. P.** (1986): Block-implicit multigrid solution of Navier-Stokes equations in primitive variables. *J. Comp. Phys.*, Vol. 65, No. 1, pp. 138-158.

**Voronoi, G.** (1908): Nouvelles applications des paramétrés continus à la théorie des formes quadratiques. Deuxième memoie, recherches sur les paralleloèdres primitifs, *J. für die Reine und Angewandte Mathematik*, Vol. 134, pp. 198-287.

**Weatherill, N. P.** (1992): Delaunay Triangulation in Computational Fluid Dynamics, *Computers Math. Applic.*, Vol. 24, No. 5-6, pp. 129-150.

**Ye, T.; Mittal, R.; Udaykumar, H. S.; Shyy, W.** (1999): An accurate Cartesian grid method for viscous incompressible flows with complex immersed boundaries. *J. Comp. Phys.*, Vol. 156, No. 2, pp. 209-240.

**Young, D. L.; Lane, S. C.; Lin, C. Y.; Chiu, C. L.; Chen, K. C.** (2004): Solutions of 2D and 3D Stokes laws using multiquadrics method. *Engr. Anal. With Bound. Elem.*, Vol. 28, No. 10, pp. 1233-1243.

